Research Square

Preprints are preliminary reports that have not undergone peer review.
They should not be considered conclusive, used to inform clinical practice,
or referenced by the media as validated information.

Periodic Parametric Modulation and Redistribution of Quantum Resources in a Kerr Cavity under Intrinsic Decoherence

Syed Jamal Anwar

sjamalanwar@gmail.com

Quaid-i-Azam University

S. Abdul Khali S. Abdul Khali

Taif University

M.S. Ateto M.S. Ateto

South Valley University

S.M. Abo-Dahab S.M. Abo-Dahab

South Valley University

Research Article

Keywords:

Posted Date: November 17th, 2026

DOI: https://doi.org/10.21203/rs.3.rs-11612635/v1

License: This work is licensed under a Creative Commons Attribution 4.0 International License.
Read Full License

Additional Declarations: No competing interests reported.

Periodic Parametric Modulation and Redistribution of Quantum Resources in a Kerr Cavity under Intrinsic Decoherence

S. Jamal Anwar*

Department of Physics, Quaid-i-Azam University, Islamabad 45320, Pakistan

S. Abdel-Khalek†

Department of Mathematics and Statistics,

College of Science, Taif University,

P.O. Box 11099, Taif 21944, Saudi Arabia

M.S. Ateto‡ and S.M. Abo-Dahab§

Mathematics Department, Faculty of Science at Qena,

South Valley University, 83523 Qena, Egypt

(Dated: November 4, 2026)

Abstract

We investigate a two-atom Kerr cavity subjected to a periodically modulated degenerate parametric pump and intrinsic decoherence. The model is formulated in a common frame rotating at half the pump frequency for both the field and atoms, so the linear terms appear as detunings and the Kerr interaction is written in its standard form $\chi a^{\dagger 2} a^2$. A time-local extension of Milburn intrinsic decoherence is used for the driven problem and is compared with a second prescription in which only the static Hamiltonian generates the double-commutator dephasing. All principal numerical calculations use a converged Fock basis with photon cutoff $n_c = 9$, and both photon-cutoff and time-step convergence are reported. The normalized quantum Fisher information (QFI) for the initial atomic angle, together with negativity and l_1 coherence, is analyzed. The normalization $\widetilde{F}_\theta(t) = F_\theta(t)/F_\theta(0)$ makes every QFI trajectory start from unity while preserving the physical ordering and data-processing bound. Periodic modulation changes the timing and distribution of these resources, but for the baseline parameters it does not exceed the unmodulated case in late-time averaged normalized QFI. The raw initial-angle QFI remains below its analytically determined initial value, while the plotted normalized QFI satisfies $\widetilde{F}_\theta(t) \leq 1$, as required by data processing. The results therefore establish a numerically converged description of quantum-resource redistribution rather than a generic claim of modulation-induced protection.

Keywords: periodic parametric modulation; Kerr cavity; Tavis–Cummings model; intrinsic decoherence; quantum Fisher information; entanglement; coherence

*Electronic address: sjamalanwar@gmail.com

†Electronic address: sabotalb@tu.edu.sa

‡Electronic address: mohamed.ali11@sci.svu.edu.eg

§Electronic address: elsayed.khodeari@sci.svu.edu.eg

I. INTRODUCTION

Quantum technologies depend on the ability to prepare, preserve and read out nonclassical states in situations where the system is never perfectly isolated. Entanglement, discord-type correlations and coherence provide different views of this nonclassicality, while quantum Fisher information (QFI) connects the state directly with the precision that can be achieved in parameter estimation [1–16]. These quantities do not respond to noise in the same way. A state may lose entanglement rapidly while retaining discord or coherence, and a state with visible correlations does not automatically provide the best metrological sensitivity. For this reason, it is useful to study correlation measures and QFI together rather than treating them as interchangeable indicators of quantum performance.

Cavity and circuit quantum electrodynamics provide particularly clean settings for this purpose. The Jaynes-Cummings and Tavis-Cummings models describe the coherent exchange of excitations between one or many two-level systems and a quantized field [17–23]. Their basic structure appears in atomic cavities, superconducting circuits and related hybrid platforms [38–43]. Even in the simplest resonant case, the discrete spectrum of the field produces collapse-revival dynamics and strong atom-field correlations. Once nonlinear optical processes are introduced, the same models acquire a much richer spectrum and can support new interference pathways that are useful for state engineering and sensing.

Two nonlinear ingredients are especially relevant here. The Kerr interaction produces an intensity-dependent phase shift and therefore changes the relative phases accumulated by different photon-number components [32–37]. Parametric amplification, in contrast, creates or annihilates photons in pairs and is closely connected with squeezing and phase-sensitive amplification [25–30]. These processes can reinforce each other, but they can also compete. A stronger pump does not necessarily mean a better quantum resource: it can populate a wider part of Hilbert space, redistribute coherence and make a reduced atomic state more sensitive to dephasing. The useful operating point is therefore expected to depend on the balance between atom-field coupling, Kerr strength and parametric drive.

Decoherence adds another layer to this balance. Standard open-system descriptions attribute decoherence to coupling with external degrees of freedom [47–54]. Milburn proposed a different phenomenological mechanism in which the system undergoes a stochastic sequence of unitary steps generated by its own Hamiltonian [31]. In the continuous-time approxima-

tion this produces a double-commutator term and suppresses coherences between energy eigenstates at a rate proportional to the square of their energy separation. The model is simple enough for controlled numerical work but nontrivial enough to reveal how nonlinear spectra influence the survival of quantum resources.

Recent studies have combined multipartite atom-field interactions, Kerr nonlinearity and intrinsic decoherence to examine global quantum discord and QFI [67–70]. Those studies show that system size, nonlinear strength and parametric amplification can change the amplitude and lifetime of quantum correlations, and that the behavior of QFI need not follow the behavior of discord. They also make clear that static parameter scans leave an important control question open. In most calculations the parametric pump is taken to be constant. In an experiment, however, the pump amplitude is a controllable quantity, and deliberately modulating it introduces a new time scale that can be compared with the coherent atom-field exchange and with the nonlinear phase accumulation.

Periodic driving is attractive because it can reshape dynamics without adding a new quantum subsystem. Instead of asking only whether a fixed value of the amplification strength is favorable, one can ask whether a time-dependent drive can move the system repeatedly through regions of Hilbert space in which the reduced atomic state retains useful sensitivity. This is a Floquet-control problem in a broad sense: the Hamiltonian is periodic, but the quantity of interest is not merely a quasienergy spectrum. We are interested in the actual time-dependent quantum resources after the field has been traced out. The competition between the modulation frequency, modulation depth, Kerr phase and intrinsic-decoherence rate can therefore produce control windows that are invisible in a static calculation.

The metrological aspect requires particular care. QFI is monotonic under parameter-independent quantum channels, so an evolution that does not itself depend on the estimated parameter cannot create unlimited information about a parameter encoded only in the initial state [8–16]. In the present work the estimated parameter is the initial atomic mixing angle, and the numerical derivative is taken after propagating neighboring initial states through exactly the same dynamical map. This construction provides an internal consistency check and prevents an artificial increase of QFI caused by inconsistent differentiation. Negativity and the l_1 norm of coherence are evaluated alongside QFI because they reveal whether a favorable metrological window is accompanied by entanglement, by single-basis coherence, or by neither [55–59].

The central question of this paper is therefore how a periodically modulated parametric amplifier redistributes useful atomic information under intrinsic decoherence, and which modulation frequencies and depths give the most favorable compromise among QFI, entanglement and coherence. We answer this question for two atoms coupled to a truncated single-mode cavity with Kerr nonlinearity. We compare constant and modulated pumping, scan the modulation frequency and depth, and use late-time averages to distinguish persistent behavior from short transient revivals. The photon cutoff is treated only as a numerical convergence parameter, not as a physical source of photons.

The main result is that modulation is not uniformly beneficial. In the baseline parameter set, the unmodulated pump gives the largest late-time averaged QFI, while low-to-intermediate modulation frequencies can still produce substantial transient redistribution and selected intervals of larger reduced-state QFI or negativity. Increasing modulation depth beyond the weak-drive limit generally lowers the late-time averaged normalized QFI. The physically defensible conclusion is therefore control and redistribution, not universal protection. This distinction is important because it separates a real dynamical modulation effect from an overstated metrological advantage.

The paper is organized as follows. Section 2 introduces the driven Kerr-parametric Tavis-Cummings model and the intrinsic-decoherence prescriptions. Section 3 defines QFI, negativity and coherence and presents the numerical results with convergence tests. Section 4 gives the physical interpretation and limitations, and Section 5 summarizes the conclusions and possible extensions.

Three methodological points are essential for a controlled nonlinear-cavity calculation. First, the parametric-amplifier Hamiltonian is derived in the pump rotating frame, which removes ambiguity between the bare cavity frequency and the pump detuning. Second, numerical convergence is tested explicitly because a two-photon drive can populate field states far above a very small Fock cutoff. Third, for a time-dependent Hamiltonian we distinguish the adopted time-local Milburn extension from the original static construction and test the sensitivity of the conclusions to that modeling choice. These checks turn the modulation problem into a reproducible control calculation rather than a parameter scan based on an undersized Hilbert space.

II. MODEL AND THEORETICAL FRAMEWORK

The physical configuration of the proposed two-atom Kerr cavity, including its periodically modulated parametric drive and intrinsic decoherence, is illustrated in Fig. 1.

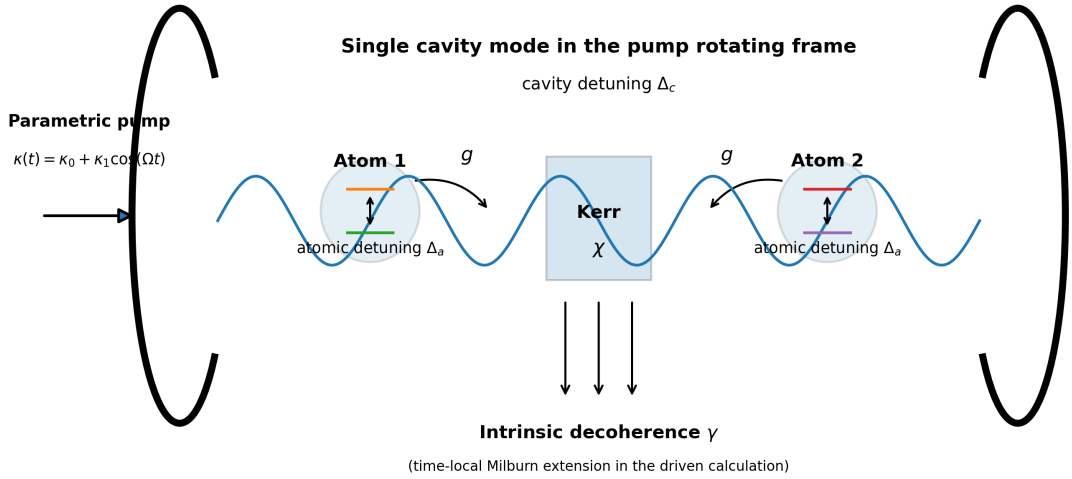


FIG. 1: Schematic of the periodically driven nonlinear cavity in the pump rotating frame. Two identical two-level atoms with atomic detuning Δ_a interact with a single cavity mode of detuning Δ_c through coupling g. The cavity contains a Kerr medium of strength χ, is driven by $\kappa(t) = \kappa_0 + \kappa_1 \cos(\Omega t)$, and is subjected to the time-local intrinsic-decoherence model with coefficient γ.

A. Pump rotating frame and Hamiltonian

We consider N identical two-level atoms interacting with one quantized cavity mode. The atom-field part follows the Tavis–Cummings construction [18, 19], while the Kerr and degenerate parametric terms follow standard nonlinear-optical models [22, 26]. Throughout, natural units with $\hbar = 1$ are used. In the laboratory frame, a degenerate parametric pump at angular frequency ω_p carries an explicit phase factor. A convenient form is

$$H_{\mathrm{PA}}^{\mathrm{lab}}(t) = \frac{i}{2}\left[\epsilon(t) a^{\dagger 2} e^{-i\omega_p t} - \epsilon^*(t) a^2 e^{i\omega_p t}\right]. \tag{1}$$

To remove the pump phase consistently from both the field and atom-field interaction,

we transform the complete atom-field system with

$$U(t) = \exp\left[-i\frac{\omega_p t}{2}\left(a^\dagger a + \frac{1}{2}\sum_j \sigma_z^{(j)}\right)\right]. \tag{2}$$

This common rotating frame converts the bare cavity and atomic frequencies into the detunings $\Delta_c = \omega_c - \omega_p/2$ and $\Delta_a = \omega_0 - \omega_p/2$ while leaving the rotating-wave atom-field coupling stationary. The full rotating-frame Hamiltonian is

$$H(t) = \Delta_c a^\dagger a + \sum_{j=1}^{N}\frac{\Delta_a}{2}\sigma_z^{(j)} + g\sum_{j=1}^{N}\left(a\sigma_+^{(j)} + a^\dagger\sigma_-^{(j)}\right) + \chi a^{\dagger 2}a^2 + \frac{i\kappa(t)}{2}\left(a^{\dagger 2} - a^2\right). \tag{3}$$

Here a ($a^\dagger$) annihilates (creates) a cavity photon, $\sigma_z^{(j)}$ is the inversion operator of atom j, and $\sigma_\pm^{(j)}$ are its ladder operators. The standard Kerr interaction $\chi a^{\dagger 2}a^2 = \chi n(n-1)$ is used rather than χn^2; the two forms differ by a linear shift χn, which would otherwise have to be absorbed into Δ_c. The pump envelope is

$$\kappa(t) = \kappa_0 + \kappa_1\cos(\Omega t). \tag{4}$$

The numerical results below are evaluated at pump-frame resonance, $\Delta_c = \Delta_a = 0$, so all frequencies are scaled by g. The total Hilbert space is $\mathcal{H}_A \otimes \mathcal{H}_F$ with $\dim(\mathcal{H}_A) = 2^N$ and $\mathcal{H}_F = \mathrm{span}\{|0\rangle, \ldots, |n_c\rangle\}$. Because the two-photon term couples $|n\rangle$ to $|n \pm 2\rangle$, convergence with n_c must be verified rather than interpreted as a physical photon-number control parameter.

B. Initial state and analytic parameter derivative

The two atoms are prepared in a partially mixed Bell-like state and the cavity starts in vacuum. The encoded parameter is the preparation angle θ, not a Hamiltonian parameter:

$$\rho_A(0) = (1-p)|\psi_\theta\rangle\langle\psi_\theta| + p|gg\rangle\langle gg|, \qquad |\psi_\theta\rangle = \cos\theta|gg\rangle + \sin\theta|ee\rangle. \tag{5}$$

$$\rho(0) = \rho_A(0)\otimes|0\rangle\langle 0|, \qquad \partial_\theta\rho_A(0) = (1-p)\left(|\psi_\theta'\rangle\langle\psi_\theta| + |\psi_\theta\rangle\langle\psi_\theta'|\right), \tag{6}$$

with $|\psi_\theta'\rangle = -\sin\theta|gg\rangle + \cos\theta|ee\rangle$. Propagating ρ and $\partial_\theta\rho$ through the same θ-independent channel avoids numerical differentiation artifacts. We use $p = 0.30$ and $\theta = \pi/4$.

C. Intrinsic decoherence for a driven Hamiltonian

For a static Hamiltonian, Milburn intrinsic decoherence [31] leads to a double commutator in the Hamiltonian. For the periodically driven case we explicitly adopt a time-local extension in which the instantaneous Hamiltonian enters the generator:

$$\dot{\rho} = -i[H(t), \rho] - \frac{\gamma}{2}[H(t), [H(t), \rho]]. \tag{7}$$

This equation is a well-defined time-local completely positive generator with instantaneous Lindblad operator $L(t) = \sqrt{\gamma}\, H(t)$, but it should be regarded as an extension of the original static Milburn construction rather than as an automatic consequence of it. To test the model dependence, we also calculate a comparison prescription in which the coherent evolution is generated by $H(t)$ while the double commutator contains only the static part $H_0 = H(t)|_{\kappa_1=0}$:

$$\dot{\rho} = -i[H(t), \rho] - \frac{\gamma}{2}[H_0, [H_0, \rho]]. \tag{8}$$

The comparison is reported in Fig. 8. This distinction is particularly relevant at high Ω because the instantaneous-H prescription contains terms proportional to $\cos^2(\Omega t)$, whose time average does not vanish.

D. Reduced state and quantum resources

$$\rho_A(t) = \mathrm{Tr}_F\, \rho(t). \tag{9}$$

The QFI of the reduced atomic state with respect to θ is evaluated from its spectral decomposition $\rho_A = \sum_m \lambda_m |m\rangle\langle m|$:

$$F_\theta = 2 \sum_{m,n:\, \lambda_m+\lambda_n>0} \frac{|\langle m|\partial_\theta \rho_A|n\rangle|^2}{\lambda_m + \lambda_n}. \tag{10}$$

For the chosen initial mixed state, the analytic raw value is $F_\theta(0) \approx 2.38$. To present all metrological curves on a common unit scale, we use the normalized QFI

$$\widetilde{F}_\theta(t) = \frac{F_\theta(t)}{F_\theta(0)}, \tag{11}$$

so that $\widetilde{F}_\theta(0) = 1$. Since the subsequent evolution and the partial trace are θ-independent quantum channels, the data-processing inequality requires $F_\theta(t) \leq F_\theta(0)$, equivalently $\widetilde{F}_\theta(t) \leq 1$, at all times. This serves as a strict numerical validation test. All QFI figures and late-time QFI averages reported below use $\widetilde{F}_\theta$; the unnormalized value is retained internally in the code for the monotonicity check. Two-atom negativity and basis-dependent l_1 coherence are

$$\mathcal{N} = \frac{\|\rho_A^{T_2}\|_1 - 1}{2}, \qquad C_{l_1} = \sum_{i \neq j} |(\rho_A)_{ij}|. \tag{12}$$

E. Numerical propagation and convergence

All frequencies are scaled by the atom–field coupling g, and time is reported as the dimensionless variable gt. Unless varied, $\chi/g = 0.35$, $\kappa_0/g = 0.70$, $\kappa_1/g = 0.45$, $\Omega/g = 0.80$, $\gamma g = 0.025$, $p = 0.30$, $\theta = \pi/4$, and $n_c = 9$. Here γ multiplies the double commutator and therefore has dimensions of time when H is written in frequency units; consequently γg is the dimensionless intrinsic- decoherence strength. The coupled equations for ρ and $\partial_\theta \rho$ are integrated with the classical fourth-order Runge–Kutta (RK4) method using the same time-dependent generator at every RK stage. Hermiticity and unit trace are restored only against accumulated floating-point roundoff after each full step; no positivity projection is applied. The main calculations use $\Delta(gt) = 0.01$. The derivative $\partial_\theta \rho$ is propagated through the same θ-independent linear dynamics. Photon-basis convergence was checked for $n_c = 3, 5, 7, 9$; $n_c = 7$ and 9 are already nearly indistinguishable. Time-step convergence was independently checked with $\Delta(gt) = 0.04$, 0.02 and 0.01 over the full interval $0 \leq gt \leq 30$; the three normalized-QFI trajectories overlap on the scale of the plotted curves, as shown in Fig. 9.

III. RESULTS AND DISCUSSION

A. Discussion of Figure 2: QFI under periodic modulation

The normalized QFI starts from unity for both curves and never exceeds 1, confirming the required data-processing behavior. The corresponding raw initial value is $F_\theta(0) \approx 2.38$.

Periodic pumping changes the timing and height of reduced-state revivals without creating information globally. For the baseline parameters, the constant-pump curve is higher through most of the late-time evolution, whereas the periodically modulated case exceeds it only over limited transient windows at earlier and intermediate times. This behavior is consistent with the modulation-depth scan, where the zero-modulation point gives the largest late-time averaged normalized QFI. The effect should therefore be understood as a redistribution of the initially encoded information between the atoms and the cavity, not as generation or generic protection of Fisher information.

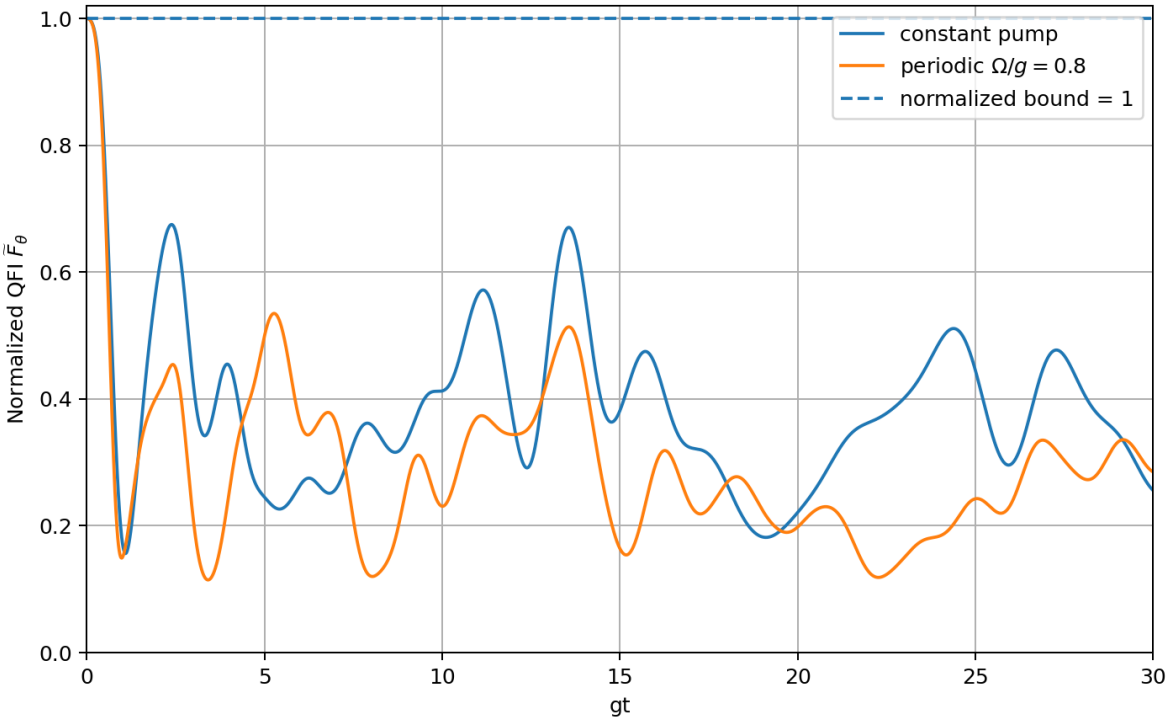


Figure 2. Normalized reduced atomic QFI $\widetilde{F}_\theta = F_\theta/F_\theta(0)$ for constant and periodically modulated parametric pumping. The dashed line at unity is the analytic initial-state bound.

B. Discussion of Figure 3: Two-atom entanglement

Negativity is more fragile than QFI and undergoes repeated suppression and revival. The periodic drive can prolong some entangled intervals, but the improvement is not uniform in time. This difference from QFI is expected because QFI for the preparation angle can remain finite in mixed atomic states that are weakly or not detectably entangled by partial transposition.

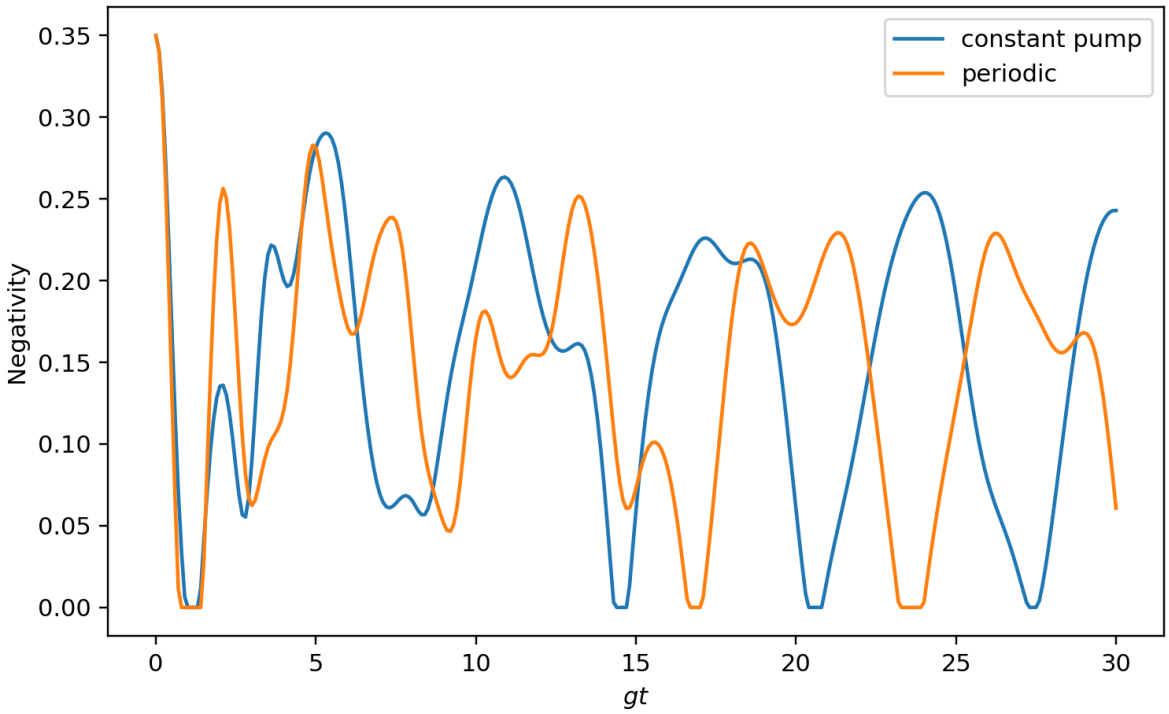


Figure 3. Two-atom negativity for constant and periodically modulated pumping.

C. Discussion of Figure 4: Atomic coherence

The l_1 coherence follows the drive-induced redistribution of off-diagonal atomic matrix elements. It generally survives over broader time windows than negativity. The comparison of Figs. 2-4 shows that no single modulation setting simultaneously maximizes all resources; QFI, negativity, and basis coherence respond to different features of the reduced state.

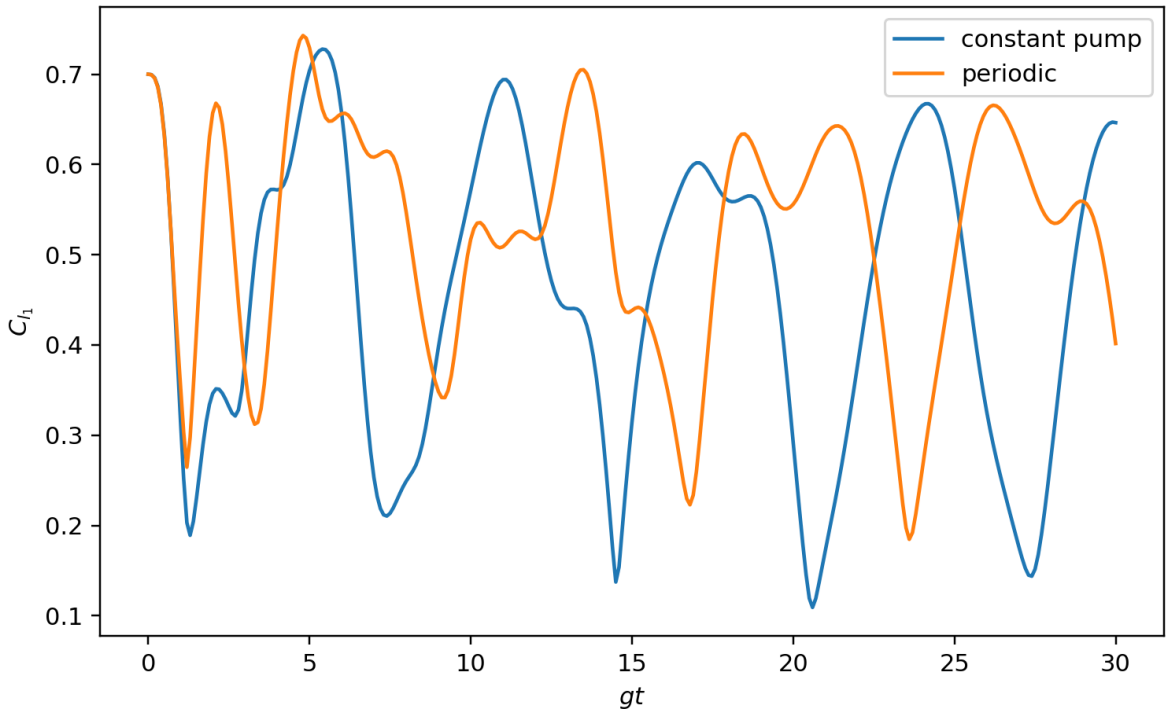


Figure 4. l_1 coherence of the reduced two-atom state.

D. Discussion of Figure 5: Modulation-frequency scan

The frequency scan reveals a low-frequency region in which the periodically driven cases retain more late-time QFI than faster modulation. This comparison is among modulated cases and should not be confused with an advantage over the unmodulated reference. For the baseline parameters, the zero-modulation point remains superior in the modulation-depth scan. The late-time averaged normalized QFI is largest for Ω/g below about unity and drops strongly as the modulation becomes faster, while negativity shows the same broad trend but is suppressed more rapidly. In the time-local intrinsic-decoherence prescription, fast modulation also enters the dephasing generator through $H(t)$, so the high-frequency suppression is not interpreted as a purely coherent Floquet-averaging effect.

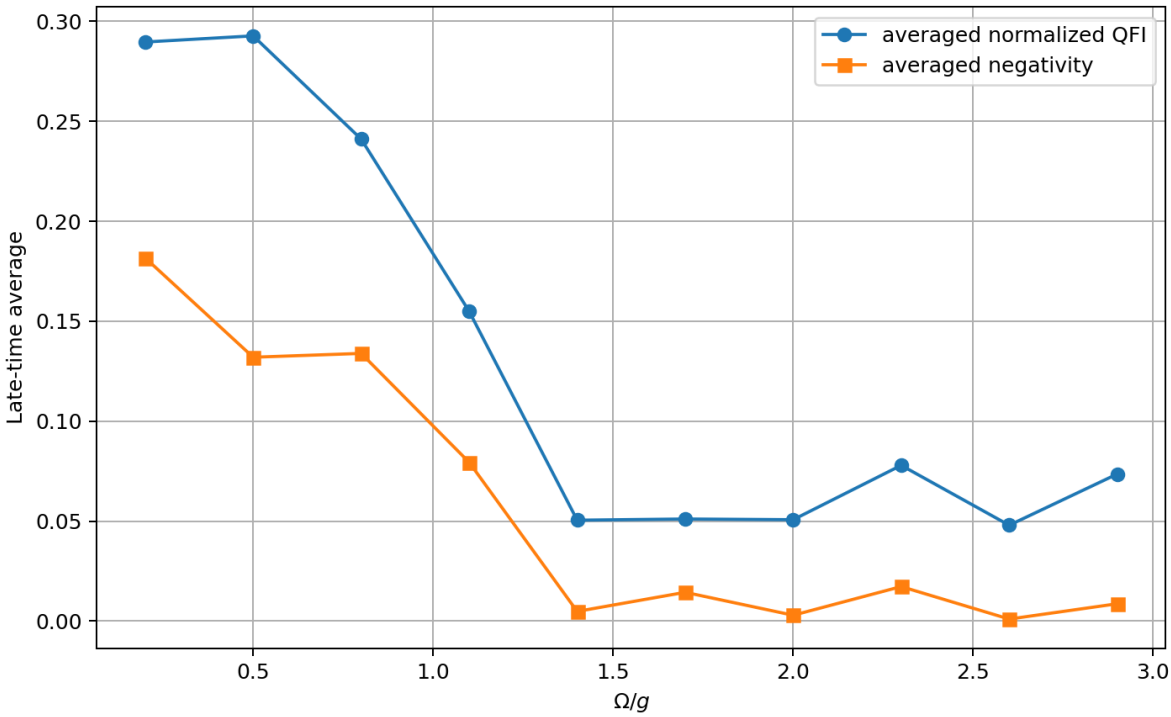


Figure 5. Late-time averaged normalized QFI and negativity versus modulation frequency for n_c=9.

E. Discussion of Figure 6: Modulation-depth scan

The modulation-depth scan shows that, for Ω/g=0.8 and the baseline Kerr and decoherence parameters, the late-time averaged normalized QFI decreases as κ_1 is increased from zero. Negativity exhibits only modest non-monotonic structure and does not establish a simultaneous metrological advantage. Thus the numerical evidence supports dynamical redistribution and transient control, but not generic late-time protection by deeper modulation. The need for a converged Fock basis becomes more important as κ_1 increases because stronger pair creation populates higher photon-number sectors.

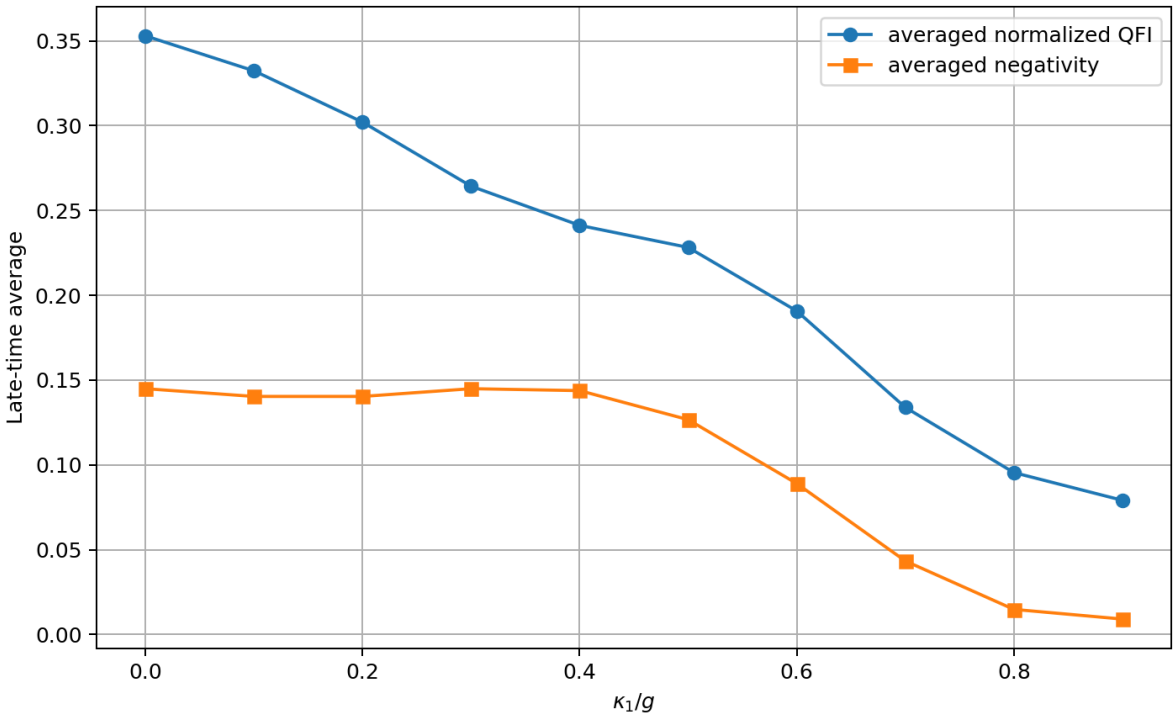


Figure 6. Late-time averaged normalized QFI and negativity versus modulation depth κ_1/g at Ω/g=0.8.

F. Discussion of Figure 7: Photon-cutoff convergence

The cutoff test demonstrates that n_c is a numerical convergence parameter rather than a physical photon-number knob. The n_c=3 result differs visibly from the converged calculation, while n_c=7 and n_c=9 lie close over the displayed interval. All principal figures therefore use n_c=9. This correction removes the artificial cutoff dependence that can otherwise be mistaken for a physical transition.

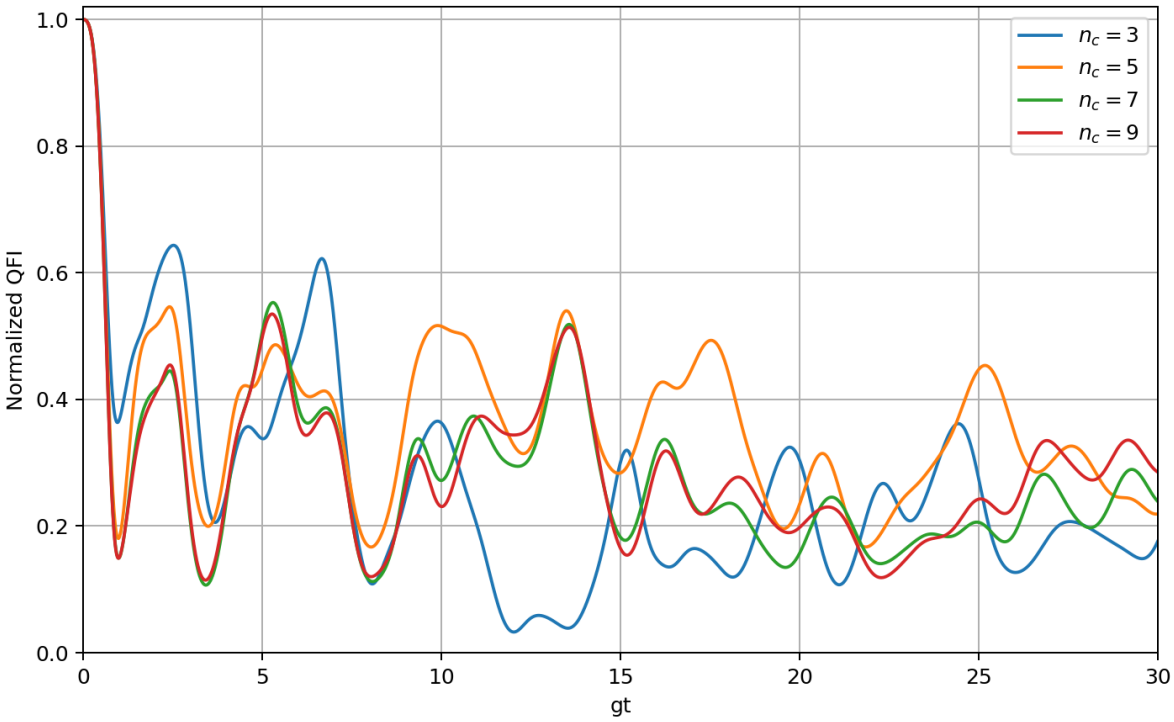


Figure 7. Normalized-QFI convergence with photon cutoff n_c.

G. Discussion of Figure 8: Dependence on the intrinsic-decoherence prescription

The two curves share the same initial condition but differ quantitatively because the modulated part of $H(t)$ contributes directly to the double commutator only in the instantaneous-H prescription. The comparison makes the modeling assumption transparent. The existence of controlled QFI redistribution survives qualitatively, but precise optimal frequencies and amplitudes should not be regarded as universal until a microscopic decoherence model is specified.

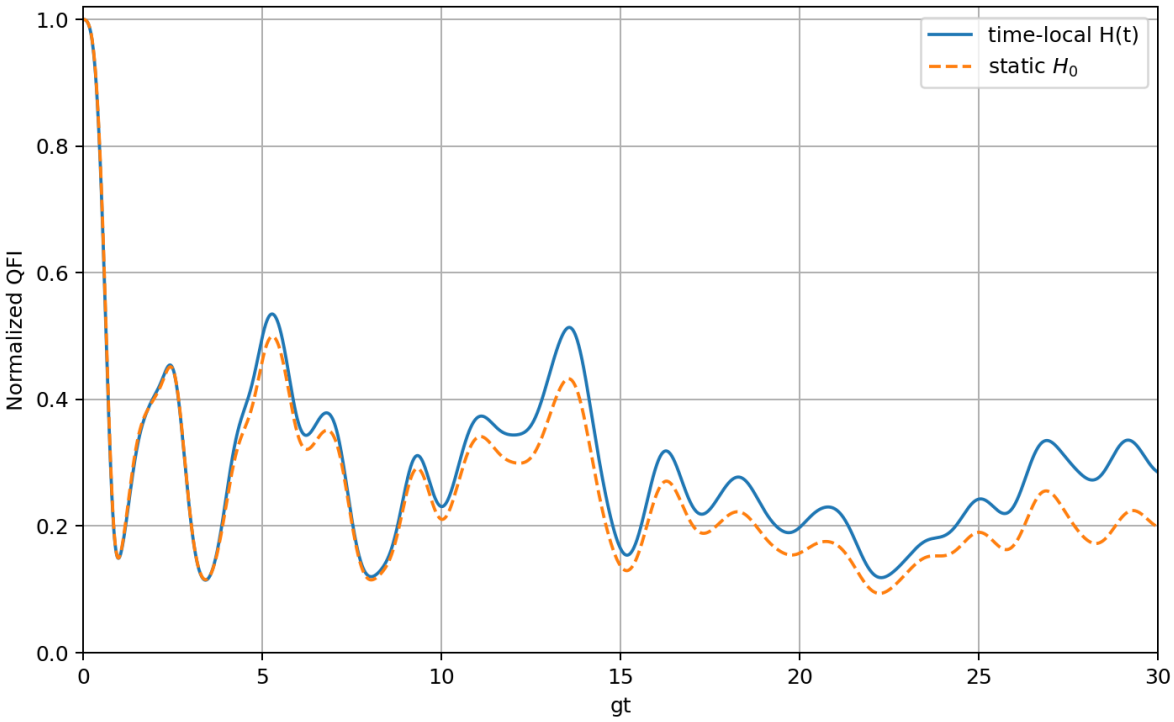


Figure 8. Normalized QFI obtained with the instantaneous-H time-local dephasing model and with a static-H_0 dephasing prescription.

H. Discussion of Figure 9: Time-step convergence

The RK4 propagation was repeated with $\Delta(gt) = 0.04$, 0.02 and 0.01 without changing any physical parameter. Figure 9 shows the complete $0 \leq gt \leq 30$ normalized-QFI trajectories rather than only a scalar late-time average. The three curves are nearly indistinguishable on the plotted scale, including the late-time interval used for averaging, showing that the reported temporal structure is not a time-discretization artifact. We therefore use $\Delta(gt) = 0.01$ in all principal driven calculations.

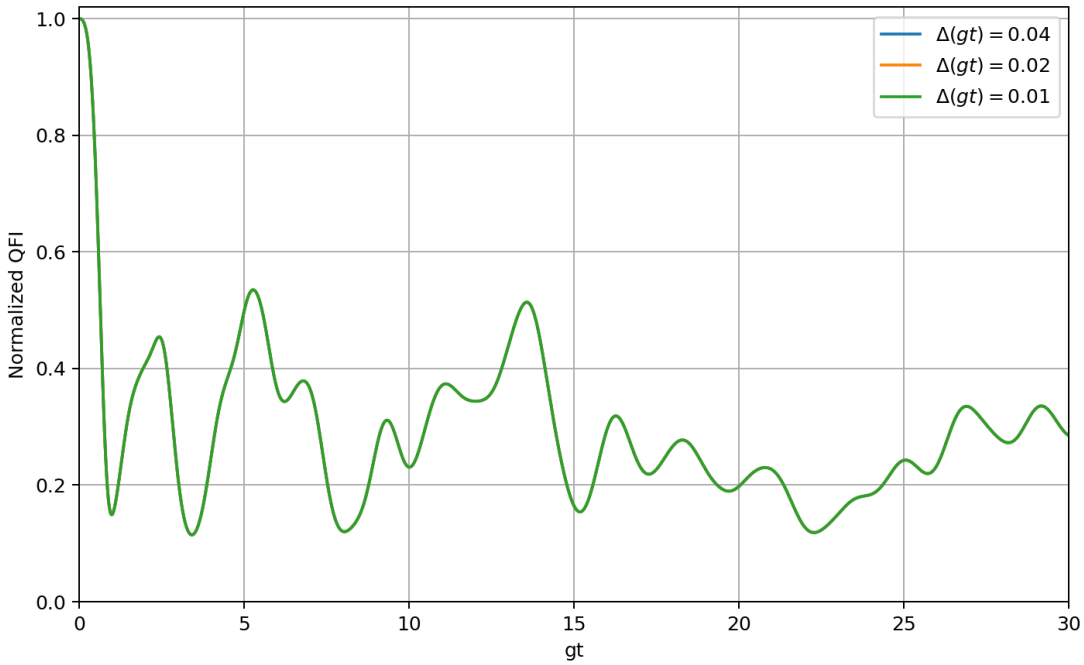


Figure 9. Time-step convergence of the normalized reduced atomic QFI for the baseline periodically driven case at n_c=9.

IV. PHYSICAL INTERPRETATION, LIMITATIONS, AND SCOPE

Periodic modulation of a degenerate parametric amplifier changes the occupation and phase structure of the even-photon sectors of the cavity. The Kerr term makes these sectors acquire number-dependent phases, while the Tavis-Cummings coupling transfers the resulting field structure to the two atoms. The observed QFI control is therefore a reduced-state localization effect. It does not violate QFI monotonicity because the total channel is independent of θ and the raw atomic QFI always remains below its initial value, equivalently $\widetilde{F}_\theta \leq 1$.

The model remains idealized. Ordinary cavity leakage, atomic spontaneous emission, finite pump phase noise, and thermal photons are not included. The time-dependent intrinsic-decoherence generator is phenomenological, so the comparison in Fig. 8 is included to separate robust qualitative conclusions from prescription-dependent quantitative ones. A future experimental model should combine the present coherent Hamiltonian with independently calibrated Lindblad channels.

V. CONCLUSIONS

The periodically driven Kerr-Tavis-Cummings model is formulated in a consistent pump rotating frame with the standard Kerr interaction
$chia^{dagger2}a^2$, a converged Fock basis, and an explicit time-local extension of Milburn intrinsic decoherence. The calculations show that periodic two-photon modulation redistributes preparation-angle information and atomic correlations, but the baseline parameter set does not support a general claim that modulation protects the late-time averaged normalized QFI better than the constant-pump case. Low-to-intermediate modulation frequencies remain useful for reshaping transient revivals and for controlling when information is localized in the atomic subsystem. Photon-cutoff and time-step convergence, together with the comparison of two intrinsic-decoherence prescriptions, make these conclusions numerically and conceptually reproducible.

Declarations

Author contributions. S. Jamal Anwar: conceptualization, methodology, investigation, numerical analysis, visualization, writing–original draft, and writing–review and editing. S. Abdel-Khalek: methodology, validation, interpretation, supervision, and writing–review and editing. M.S. Ateto: manuscript writing and critical reviewing. S.M. Abo-Dahab: manuscript writing and critical reviewing.

Funding. The authors declare that no specific funding was received for this work.

Data availability. No external data sets were generated or analyzed in this study. The results reported in this article are based on the theoretical model and numerical calculations described in the manuscript.

Code availability. The MATLAB codes used for the numerical calculations are available from the corresponding author upon reasonable request.

Competing interests. The authors declare that they have no competing interests or conflicts of interest.

Ethics approval. Not applicable.

Consent to participate. Not applicable.

Consent for publication. Not applicable.

Corresponding author. Correspondence should be addressed to S. Jamal Anwar (sjamalanwar@gmail.com).

---

[1] M. A. Nielsen and I. L. Chuang, Quantum Computation and Quantum Information, Cambridge University Press, Cambridge (2010).

[2] R. Horodecki, P. Horodecki, M. Horodecki and K. Horodecki, Quantum entanglement, Rev. Mod. Phys. 81, 865 (2009).

[3] H. Ollivier and W. H. Zurek, Quantum discord: a measure of the quantumness of correlations, Phys. Rev. Lett. 88, 017901 (2001).

[4] L. Henderson and V. Vedral, Classical, quantum and total correlations, J. Phys. A 34, 6899 (2001).

[5] K. Modi, A. Brodutch, H. Cable, T. Paterek and V. Vedral, The classical-quantum boundary for correlations: discord and related measures, Rev. Mod. Phys. 84, 1655 (2012).

[6] C. C. Rulli and M. S. Sarandy, Global quantum discord in multipartite systems, Phys. Rev. A 84, 042109 (2011).

[7] S. Campbell, T. J. G. Apollaro, C. Di Franco, L. Banchi, A. Cuccoli, R. Vaia, F. Plastina and M. Paternostro, Global quantum correlations in finite-size spin chains, New J. Phys. 15, 043033 (2013).

[8] S. L. Braunstein and C. M. Caves, Statistical distance and the geometry of quantum states, Phys. Rev. Lett. 72, 3439 (1994).

[9] M. G. A. Paris, Quantum estimation for quantum technology, Int. J. Quantum Inf. 7, 125 (2009).

[10] G. Toth and I. Apellaniz, Quantum metrology from a quantum information science perspective, J. Phys. A 47, 424006 (2014).

[11] L. Pezze, A. Smerzi, M. K. Oberthaler, R. Schmied and P. Treutlein, Quantum metrology with nonclassical states of atomic ensembles, Rev. Mod. Phys. 90, 035005 (2018).

[12] V. Giovannetti, S. Lloyd and L. Maccone, Advances in quantum metrology, Nat. Photonics 5, 222 (2011).

[13] C. W. Helstrom, Quantum Detection and Estimation Theory, Academic Press, New York (1976).

[14] A. S. Holevo, Probabilistic and Statistical Aspects of Quantum Theory, North-Holland, Amsterdam (1982).

[15] S. F. Huelga et al., Improvement of frequency standards with quantum entanglement, Phys. Rev. Lett. 79, 3865 (1997).

[16] R. Demkowicz-Dobrzanski, M. Jarzyna and J. Kolodynski, Quantum limits in optical interferometry, Prog. Opt. 60, 345 (2015).

[17] I. I. Rabi, On the process of space quantization, Phys. Rev. 49, 324 (1936).

[18] E. T. Jaynes and F. W. Cummings, Comparison of quantum and semiclassical radiation theories with application to the beam maser, Proc. IEEE 51, 89 (1963).

[19] M. Tavis and F. W. Cummings, Exact solution for an N-molecule-radiation-field Hamiltonian, Phys. Rev. 170, 379 (1968).

[20] H. J. Carmichael, Statistical Methods in Quantum Optics 1, Springer, Berlin (1999).

[21] C. W. Gardiner and P. Zoller, Quantum Noise, 3rd ed., Springer, Berlin (2004).

[22] D. F. Walls and G. J. Milburn, Quantum Optics, 2nd ed., Springer, Berlin (2008).

[23] M. O. Scully and M. S. Zubairy, Quantum Optics, Cambridge University Press, Cambridge (1997).

[24] R. J. Glauber, Coherent and incoherent states of the radiation field, Phys. Rev. 131, 2766 (1963).

[25] D. Stoler, Equivalence classes of minimum uncertainty packets, Phys. Rev. D 1, 3217 (1970).

[26] B. R. Mollow and R. J. Glauber, Quantum theory of parametric amplification. I, Phys. Rev. 160, 1076 (1967).

[27] B. R. Mollow and R. J. Glauber, Quantum theory of parametric amplification. II, Phys. Rev. 160, 1097 (1967).

[28] C. M. Caves, Quantum limits on noise in linear amplifiers, Phys. Rev. D 26, 1817 (1982).

[29] R. Loudon and P. L. Knight, Squeezed light, J. Mod. Opt. 34, 709 (1987).

[30] M. J. Collett and C. W. Gardiner, Squeezing of intracavity and traveling-wave light fields produced in parametric amplification, Phys. Rev. A 30, 1386 (1984).

[31] G. J. Milburn, Intrinsic decoherence in quantum mechanics, Phys. Rev. A 44, 5401 (1991).

[32] J. Kerr, A new relation between electricity and light: dielectrified media birefringent, Philos. Mag. 50, 337 (1875).

[33] P. D. Drummond and D. F. Walls, Quantum theory of optical bistability. I. Nonlinear polar-

isability model, J. Phys. A 13, 725 (1980).

[34] G. Kirchmair et al., Observation of quantum state collapse and revival due to the single-photon Kerr effect, Nature 495, 205 (2013).

[35] M. A. C. Rossi, F. Albarelli and M. G. A. Paris, Enhanced estimation of loss in the presence of Kerr nonlinearity, Phys. Rev. A 93, 053805 (2016).

[36] A. Imamoglu, H. Schmidt, G. Woods and M. Deutsch, Strongly interacting photons in a nonlinear cavity, Phys. Rev. Lett. 79, 1467 (1997).

[37] K. M. Gheri, W. Alge, P. Grangier and A. Zeilinger, Quantum analysis of the photonic blockade mechanism, Phys. Rev. A 60, R2673 (1999).

[38] A. Blais, R.-S. Huang, A. Wallraff, S. M. Girvin and R. J. Schoelkopf, Cavity quantum electrodynamics for superconducting electrical circuits: an architecture for quantum computation, Phys. Rev. A 69, 062320 (2004).

[39] A. Blais, A. L. Grimsmo, S. M. Girvin and A. Wallraff, Circuit quantum electrodynamics, Rev. Mod. Phys. 93, 025005 (2021).

[40] H. Walther, B. T. H. Varcoe, B.-G. Englert and T. Becker, Cavity quantum electrodynamics, Rep. Prog. Phys. 69, 1325 (2006).

[41] S. Haroche and J.-M. Raimond, Exploring the Quantum: Atoms, Cavities, and Photons, Oxford University Press, Oxford (2006).

[42] I. Buluta, S. Ashhab and F. Nori, Natural and artificial atoms for quantum computation, Rep. Prog. Phys. 74, 104401 (2011).

[43] J. Q. You and F. Nori, Atomic physics and quantum optics using superconducting circuits, Nature 474, 589 (2011).

[44] A. A. Clerk et al., Introduction to quantum noise, measurement, and amplification, Rev. Mod. Phys. 82, 1155 (2010).

[45] M. Aspelmeyer, T. J. Kippenberg and F. Marquardt, Cavity optomechanics, Rev. Mod. Phys. 86, 1391 (2014).

[46] F. Marquardt and S. M. Girvin, Optomechanics, Physics 2, 40 (2009).

[47] W. H. Zurek, Decoherence, einselection, and the quantum origins of the classical, Rev. Mod. Phys. 75, 715 (2003).

[48] M. Schlosshauer, Decoherence, the measurement problem, and interpretations of quantum mechanics, Rev. Mod. Phys. 76, 1267 (2005).

[49] H.-P. Breuer and F. Petruccione, The Theory of Open Quantum Systems, Oxford University Press, Oxford (2002).

[50] A. Rivas and S. F. Huelga, Open Quantum Systems: An Introduction, Springer, Heidelberg (2012).

[51] H.-P. Breuer, E.-M. Laine, J. Piilo and B. Vacchini, Colloquium: non-Markovian dynamics in open quantum systems, Rev. Mod. Phys. 88, 021002 (2016).

[52] I. de Vega and D. Alonso, Dynamics of non-Markovian open quantum systems, Rev. Mod. Phys. 89, 015001 (2017).

[53] G. Lindblad, On the generators of quantum dynamical semigroups, Commun. Math. Phys. 48, 119 (1976).

[54] V. Gorini, A. Kossakowski and E. C. G. Sudarshan, Completely positive dynamical semigroups of N-level systems, J. Math. Phys. 17, 821 (1976).

[55] W. K. Wootters, Entanglement of formation of an arbitrary state of two qubits, Phys. Rev. Lett. 80, 2245 (1998).

[56] G. Vidal and R. F. Werner, Computable measure of entanglement, Phys. Rev. A 65, 032314 (2002).

[57] T. Baumgratz, M. Cramer and M. B. Plenio, Quantifying coherence, Phys. Rev. Lett. 113, 140401 (2014).

[58] A. Streltsov, G. Adesso and M. B. Plenio, Colloquium: quantum coherence as a resource, Rev. Mod. Phys. 89, 041003 (2017).

[59] M.-L. Hu et al., Quantum coherence and geometric quantum discord, Phys. Rep. 762-764, 1 (2018).

[60] R. A. Fisher, Theory of statistical estimation, Proc. Cambridge Philos. Soc. 22, 700 (1925).

[61] S. Luo, Wigner-Yanase skew information and uncertainty relations, Phys. Rev. Lett. 91, 180403 (2003).

[62] D. Petz and C. Ghinea, Introduction to quantum Fisher information, in Quantum Probability and Related Topics, World Scientific (2011).

[63] P. Hyllus et al., Fisher information and multiparticle entanglement, Phys. Rev. A 85, 022321 (2012).

[64] G. Toth, Multipartite entanglement and high-precision metrology, Phys. Rev. A 85, 022322 (2012).

[65] J. Ma, X. Wang, C. P. Sun and F. Nori, Quantum spin squeezing, Phys. Rep. 509, 89 (2011).

[66] L. Mandel and E. Wolf, Optical Coherence and Quantum Optics, Cambridge University Press, Cambridge (1995).

[67] M. Ibrahim, S. Jamal Anwar, S. Abdel-Khalek, M. Ramzan and M. Khalid Khan, Effects of intrinsic decoherence in multipartite system subjected to Kerr effect and parametric amplification with quantum correlations and estimation, arXiv:2509.03073 (2025).

[68] S. Almalki et al., Quantum correlations and Fisher information in multipartite two-level system under Kerr medium effect, Thermal Science 29, 347 (2025).

[69] M. Ibrahim, Nonlinear dynamics of coherent parametric amplification in multipartite two-level system under intrinsic decoherence, arXiv:2606.25860 (2026).

[70] M. Ibrahim et al., Dynamics of quantum correlations and Fisher information of a multipartite system under the Stark effect, Alexandria Eng. J. 104, 378 (2024).